11-fold Superstructure of $TaGe_{4/11}Te_2$: A Novel Response to Charge Transfer in the MA_xTe_2 (M = Nb, Ta; A = Si, Ge; $^1/_3 \leq x \leq {}^1/_2$) Series

A. van der Lee, M. Evain,* L. Monconduit, and R. Brec

IMN, Laboratoire de Chimie des Solides, UMR CNRS No. 110, Université de Nantes, 2 rue de la Houssinière, 44072 Nantes Cedex 03, France

V. Petříček

Institute of Physics, Academy of Sciences of the Czech Republic, Na Slovance 2, 180 40 Praha 8, Czech Republic

Received December 28, 1993•

The commensurately modulated structure of $TaGe_{4/11}Te_2$ was determined from single-crystal X-ray diffraction data. $TaGe_{4/11}Te_2$ is orthorhombic; the basic unit cell dimensions are a = 6.4396(8) Å, b = 14.044(2) Å, and c = 3.8522(5) Å, with Z = 4. The (3 + 1)D superspace group is $B2mm(00\gamma)$, where $\gamma = {}^4/_{11}$. The structure consists of [Te/M, A/Te] sandwiches stacked in the AA/BB mode like other MA_xTe_2 phases (M = Nb,Ta; A = Si, Ge; $^1/_3 \leq x \leq {}^1/_2$). Also, Ta and Ge are in Te trigonal-prismatic and square coordinations, respectively. The intrasandwich cationic arrangement is, however, quite distinct from the pattern found in the parent compounds. Instead of a single zigzag strip of lone Ta atoms per sandwich per unit cell, there are two such strips plus two half-strips. It is shown that the extra number of strips is needed to obtain the proper number of short intersandwich Te–Te contacts required for the electronic stabilization of the compound. In this way an incommensurate modulated structure, as occurs for $TaSi_xTe_2$ compounds, can be avoided. It is proposed that, although the average oxidation state of Te changes from 2– in $MA_{1/2}Te_2$ to $^5/_3$– in $MA_{1/3}Te_2$, equivalent Te–Te distances need not change owing to the setting up of commensurately or incommensurately ordering motifs.

Introduction

Transition-metal tellurides are in many cases quite distinct from the transition-metal sulfides and selenides because of the less electronegative character of Te. The study of binary and ternary phases has shown that Te, unlike S and Se, tends to adopt oxidation states intermediate between 1– and 2–.[1-15] For instance, Te in the metal-rich compounds[3,4] can be considered as fully reduced, whereas Te^{2-} in metal-poorer compounds[5-8] tends to be slightly oxidized to $Te^{(2-\delta)-}$. This leads to a wide range of Te–Te distances in contrast with the more "quantum"-like character of S–S and Se–Se distances. The (fractional) oxidation state of Te can be tuned by a heterocharge substitution of the cations or by a variation of the compound stoichiometry. A nice example of the former procedure is provided by Mar *et al.*[12] The latter method is discussed in this paper.

Compounds in the MA_xTe_2 series (M = Ta, Nb; A = Si, Ge; $^1/_3 \leq x \leq {}^1/_2$) have commensurately or incommensurately modulated structures due to an ordering of M and A ions over the available sites within infinite [Te/M, A/Te] sandwiches.[16-24] M cations are usually bonded to one another in such a way that the complete set of M–M pairs forms a herringbone motif. A few M atoms are not bonded to other M atoms; they form a zigzag pattern perpendicular to the running direction of the modulation wave. The concentration of these "lone" M atoms diminishes with increasing A content, and it is for this reason that the zigzag strips of lone M atoms can be considered as faults in an otherwise regular herringbone pattern. A atoms are found in a unique square coordination of Te atoms.

The hitherto investigated commensurate superstructures have in common that exactly one electron per sandwich per unit cell is transferred from Te p-orbitals to M-metal d-block bands to adjust the electron counting in $M^{3+}(A^{2+})_x(Te^{-(3+2x)/2})_2$. The assigment of the oxidation states follows from extended Hückel tight-binding band electronic structure calculations for $MA_{1/3}Te_2$ compounds.[20,25] The stoichiometry of these compounds can be written more specifically as $MA_{(1+n)/(3+2n)}Te_2$, with n = 0, 1, 2..., whereas the modulation wave vector is directly related to the following stoichiometry: $\mathbf{q} = [(1 + n)/(3 + 2n)]\mathbf{c}^*$.[22] Each

* Author to whom correspondence should be addressed.
• Abstract published in *Advance ACS Abstracts*, June 1, 1994.

(1) Böttcher, P. *Angew. Chem.* **1988**, *100*, 781–794.
(2) Liimatta, E. W.; Ibers, J. A. *J. Solid State Chem.* **1989**, *78*, 7–16.
(3) Li, J.; Hoffmann, R.; Badding, M. E.; DiSalvo, F. J. *Inorg. Chem.* **1990**, *29*, 3943–3952.
(4) Badding, M. E; DiSalvo, F. J. *Inorg. Chem.* **1990**, *29*, 3952–3954.
(5) Keane, P. M.; Ibers, J. A. *Inorg. Chem.* **1991**, *30*, 1327–1329.
(6) Keane, P. M.; Ibers, J. A. *Inorg. Chem.* **1991**, *30*, 3096–3098.
(7) Keane, P. M.; Ibers, J. A. *J. Solid State Chem.* **1991**, *93*, 291–297.
(8) Mar, A.; Ibers, J. A. *J. Chem. Soc., Dalton Trans.* **1991**, 639–641.
(9) Tremel, W. *Angew. Chem., Int. Ed. Engl.* **1991**, *30*, 840–843.
(10) Jobic, S.; Deniard, P.; Brec, R.; Rouxel, J.; Jouanneaux, A.; Fitch, A. N. *Z. Anorg. Allg. Chem.* **1991**, *589/599*, 199–215.
(11) Li, J.; Badding, M. E.; DiSalvo, F. J. *Inorg. Chem.* **1992**, *31*, 1050–1054.
(12) Mar, A.; Jobic, S.; Ibers, J. A. *J. Am. Chem. Soc.* **1992**, *114*, 8963–8971.
(13) Jobic, S.; Brec, R.; Rouxel, J. *J. Alloys Comp.* **1992**, *178*, 253–283.
(14) Canadell, E.; Jobic, S.; Brec, R.; Rouxel, J.; Whangbo, M.-H. *J. Solid State Chem.* **1992**, *99*, 189–199.
(15) Rouxel, J. *Comments Inorg. Chem.* **1993**, *14*, 207–228.
(16) Li, J.; Caroll, P. J. *Mater. Res. Bull.* **1992**, *27*, 1073–1081.
(17) Li, J.; Badding, M. E.; DiSalvo, F. J. *J. Alloys Comp.* **1992**, *184*, 257–263.
(18) Monconduit, L.; Evain, M.; Boucher, F.; Brec, R.; Rouxel, J. *Z. Anorg. Allg. Chem.* **1992**, *616*, 1–6.
(19) Monconduit, L.; Evain, M.; Brec, R.; Rouxel, J.; Canadell, E. *C. R. Acad. Sci. Paris* **1993**, *314*, 25–34.
(20) Evain, M.; Monconduit, L.; Van der Lee, A.; Brec, R.; Rouxel, J. *New J. Chem.* **1994**, *18*, 215–222.
(21) Van der Lee, A.; Evain, M.; Monconduit, L.; Brec, R.; Rouxel, J.; Petříček, V. *Acta Crystallogr., Sect. B* **1994**, *50*, 119–128.
(22) Van der Lee, A.; Evain, M.; Monconduit, L.; Brec, R; Van Smaalen, S. *J. Phys.: Cond. Matter* **1994**, *6*, 933–944.
(23) Van der Lee, A.; Evain, M.; Mansuetto, M.; Monconduit, L.; Brec, R; Rouxel, J. *J. Solid State Chem.* **1994**, in press.
(24) Evain, M.; Van der Lee, A.; Monconduit, L.; Petříček, V. *Chem. Mater.*, submitted for publication.
(25) Canadell, E.; Monconduit, L.; Evain, M.; Brec, R.; Rouxel, J.; Whangbo, M.-H. *Inorg. Chem.* **1993**, *32*, 10–12.

0020-1669/94/1333-3032$04.50/0

Table 1. Crystallographic Data for $TaGe_{4/11}Te_2$[a]

$TaGe_{0.36364}Te_2$	$M_r = 462.55$
$a = 6.4396(8)$ Å	$B2mm(00\gamma)$
$b = 14.044(2)$ Å	$T = 295$ K
$c = 3.8522(5)$ Å	$\lambda = 0.71073$ Å
$V = 348.38(8)$ Å^3	$\rho_{calcd} = 8.818$ g cm^{-3}
$q = {}^4/_{11}\,c^*$	$\mu = 532.5$ cm^{-1}
$Z = 4$	

[a] Note: The cell dimensions refer to the basic unit cell.

sandwich contains exactly one fault per sandwich per unit cell regardless the value of n. The structures may differ, however, in the way the [Te/*M*, *A*/Te] sandwiches are stacked. The pinning of one sandwich onto another takes place only at special sites of the Te surface of a sandwich, viz. exactly at those points where the intersandwich Te–Te distances are the shortest. These short intersandwich Te–Te distances are related to the aforementioned electronic transfer.[20, 25]

The compound which is discussed in this paper, $TaGe_{4/11}Te_2$, does not comply with the general formula $MA_{(1+n)/(3+2n)}Te_2$. Indeed, instead of one electron as for the latter compounds, three electrons per sandwich per unit cell are transferred to the *M*-metal d-block bands. Since the electronic transfer is related to structural features, it is expected that the intrasandwich structure, i.e. the ordering of *M* and *A* ions, of $TaGe_{4/11}Te_2$ is different from that in $MA_{(1+n)/(3+2n)}Te_2$. In addition intersandwich Te–Te distances might be different.

Here we report the synthesis of $TaGe_{4/11}Te_2$ and its structure determination using superspace group theory.[26] The intrasandwich ordering is discussed in relation with the other ordering patterns found in the MA_xTe_2 series. The sandwich stacking, which is an important factor for the electronic stabilization and a key element in the structure determination, is given special attention.

Experimental Section

Synthesis. $TaGe_{4/11}Te_2$ was obtained during an effort to synthesize $TaGe_{1/3}Te_2$. Stoichiometric amounts of the elements for the latter compound were sealed in an evacuated silica tube. The temperature of the tube was raised to 700 K at a rate of 150 K/h. After 22 days the tube was cooled to room temperature at the same rate. Very thin platelets with a metallic luster were found in the batch. SEM analysis on seven crystals yielded an average composition of $Ta_{10.4}Ge_{3.6}Te_{22}$. The determination of the Ge and Ta content was hampered by a partial overlap of their emission peaks; $CrGeTe_3$ was used as an internal standard. Weissenberg photographs were taken to select a good-quality crystal for a subsequent data collection on a graphite-monochromated Siemens P4 diffractometer. The majority of the selected crystals exhibited weak superreflections along **c*** compatible with an 11-fold superstructure along **c**. A few crystals with a 3-fold superstructure, as would be expected for a $TaGe_{1/3}Te_2$ stoichiometry, were also present. The formation of these crystals is rather sensitive to the experimental conditions like temperature gradient and duration of the synthesis. Other syntheses yielded, for example, many crystals that are truly incommensurate ($\mathbf{q}^* = 0.3544(4)\mathbf{c}^*$).

Crystallographic Data Collection. Crystallographic data are compiled in Table 1. The measured intensities were corrected for the scale variation, Lorentz, and polarization effects. A Gaussian absorption correction was applied using the program ABSORB from the XTAL software package.[27] The intensities showed a *mmm* Laue symmetry but were averaged according to a point symmetry *2mm* (see later). All further calculations have been performed with the JANA93 computing system.[28] The scattering factors for neutral atoms and the anomalous dispersion correction were taken from ref 29. All refinements were based on $|F_o|$ and performed in a full-matrix mode, using $w = 1/(\sigma^2(|F_o|) + 0.01|F_o|^2)$ as weights.

Structure Determination and Refinement. The $TaGe_{4/11}Te_2$ basic lattice metric is very similar to that of all other MA_xTe_2 compounds, but its Bravais class is not primitive but *B*-centered. This also holds for the complete diffraction pattern, i.e. main plus satellite reflections. When first-order reflections are defined as being the strongest satellites, the wave vector describing the modulation is $\mathbf{q} = {}^4/_{11}\mathbf{c}^*$. Since the wave vector is commensurate with respect to the basic lattice, standard crystallographic techniques could be used to solve and refine the structure in an 11-fold supercell. However, it is advantageous to use superspace group theory[26] to describe the symmetry of the modulated phase. Contrary to the conventional approach, the superspace group analysis naturally divides the complete structure into a basic part and a modulated part, analogous to what is seen in the diffraction pattern. Functions are added to the structure factor expression that describe the modulations of the atoms with respect to the basic positions. In the present case these functions are expanded in a Fourier series:

$$P^{\nu}(\bar{x}_4) = P^{\nu}_0 + \sum_{n=1}^{5}[P^{\nu}_{s,n}\sin(2\pi n\bar{x}_4) + P^{\nu}_{c,n}\cos(2\pi n\bar{x}_4)]$$

$$\mathbf{r}^{\nu}(\bar{x}_4) = \mathbf{r}^{\nu}_0 + \sum_{n=1}^{5}[\mathbf{u}^{\nu}_{s,n}\sin(2\pi n\bar{x}_4) + \mathbf{u}^{\nu}_{c,n}\cos(2\pi n\bar{x}_4)]$$

where ν counts the independent atoms in the basic unit cell. The argument of the modulation function has been defined as follows: $\bar{x}_4 = t + \mathbf{q}\cdot\mathbf{r}^{\nu}_{0,L} = t + \mathbf{q}\cdot(\mathbf{r}^{\nu}_0 + \mathbf{L})$, with t being the global phase of the modulation wave ($t = 0$ is used in the present work), L being a basic structure lattice translation, and $\mathbf{u}^{\nu}_{s,n} = (A^{\nu}_{x,s,n}, A^{\nu}_{y,s,n}, A^{\nu}_{z,s,n})$, $\mathbf{u}^{\nu}_{c,n} = (A^{\nu}_{x,c,n}, A^{\nu}_{y,c,n}, A^{\nu}_{z,c,n})$. P^{ν}_0 and $\mathbf{r}^{\nu}_0$ are the basic site occupancy factor and the basic structure position, respectively. The goal of the determination of the modulated structure is the finding and the refinement of the Fourier amplitudes $P^{\nu}_{s,n}$, $P^{\nu}_{c,n}$, $\mathbf{u}^{\nu}_{s,n}$, and $\mathbf{u}^{\nu}_{c,n}$. Since the modulation is one-dimensional, the symmetry of the modulated phase can be described by a (3 + 1)D Bravais class and a (3 + 1)D superspace group.[26] The (3 + 1)D Bravais class is determined from the metric of the diffraction pattern; it is characterized by the symbol $mmmB(00\gamma)$. The determination of the superspace group symmetry follows from the systematic extinction conditions and a successful refinement of a starting model. First the basic structure is determined and refined, followed by that of the modulated structure.

The basic structure contains two independent Ta atoms per sandwich, denoted Ta(1) and Ta(2) whose positions are too close to each other to be occupied simultaneously in the real modulated structure. The sum of the occupancy probabilities of these sites in the basic structure equals 1.0. There is one Ge atom whose basic structure site occupancy was hitherto always found to match the relative magnitude (γ) of the wave vector.[20–23] Finally, one independent Te atom is present. The *B*-centering only slightly modifies the atomic positions as compared with those in the other MA_xTe_2 compounds.

The determination of the modulated structure was split into two parts. First, an appropriate model for the intrasandwich cationic ordering was sought, and then the relative stacking of the two [Te/*Ta*,*Ge*/Te] sandwiches was determined.

For the determination of the intrasandwich it was assumed that the Ta and Ge cations have the coordination they have in the other MA_xTe_2 compounds, i.e. trigonal prismatic for Ta and square for Ge.[16–24] A second assumption was that the occupation modulation wave of Ta(1) governs the relative strength of the satellite reflections. It was retrospectively found that for all other MA_xTe_2 compounds the summed squares of the *n*th-order Fourier amplitudes of the occupation wave of *M*(1) for each satellite order scale well with the mean *n*th-order satellite intensity. Thus, models for which the summed squares of the first-order Fourier amplitudes were not clearly stronger than those of the higher orders were rejected. In order to quickly cull meaningful models out of the 102 possibilities, the occupation wave was taken to be a single-block wave. Indeed if the modulation wave has only a single block, one is assured that its Fourier amplitudes approximately decrease with increasing

(26) See for a technical treatment of superspace group theory e.g. § 9.8 in: *International Tables for Crystallography*; Wilson, A. J. C., Ed.; Kluwer Academic Publishers: Dordrecht/Boston/London, 1992; Vol. C. A more descriptive treatment is given by e.g.: Janssen, T.; Janner, A. *Adv. Phys.* **1987**, *36*, 519–624. The application to MA_xTe_2 compounds is exemplified in refs 21–24.

(27) Hall, S. R., Flack, H. D., Stewart, J. M., Eds. Xtal3.2 Reference Manual. Universities of Western Australia, Geneva, and Maryland, 1992.

(28) Petříček, V. JANA93-programs for modulated and composite crystals. Institute of Physics, Praha, Czech Republic, 1993.

(29) Cromer, D. T.; Waber, J. T. In *International Tables for X-ray Crystallography*; Ibers, J. A., Hamilton, W. C., Eds.; Kynoch Press: Birmingham, England, 1974; Vol. IV, pp 72–98. Cromer, D. T. *Ibid.*, pp 149–150.

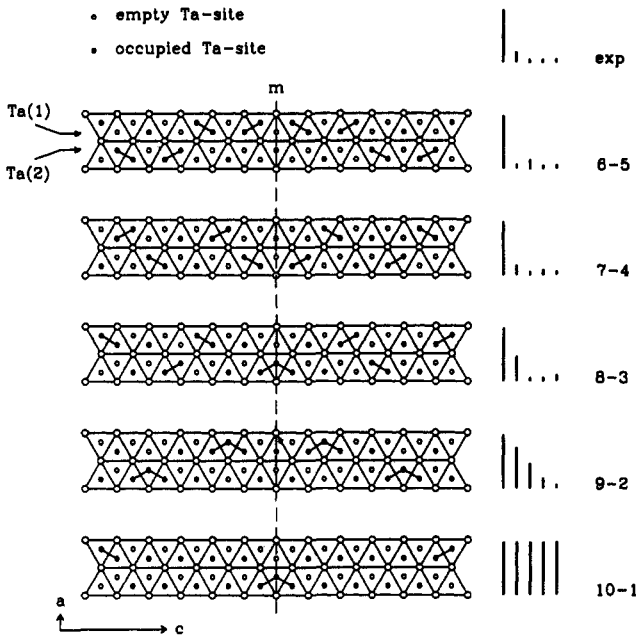

Figure 1. Most probable intrasandwich cationic arrangements for the structure of $TaGe_{4/11}Te_2$. The Ge atoms have been omitted for the sake of clarity; they are found in the middle of a "bond" of Ta vacancies. For each model the normalized intensity distribution for the different satellite orders is given, from the 1st order on the left to the 5th order on the right. The two labels of each model are derived from the numbers of occupied sites in the two indicated Ta(1) and Ta(2) rows, respectively.

order (except for very broad or small blocks). Since no *a priori* assumption could be made on the occupancy P at the Ta(1) site, other than that it should be compatible with the 11-fold superstructure, in total five models had to be considered, viz. $P^{Ta(1)} = {}^{6}/_{11}, {}^{7}/_{11}, {}^{8}/_{11}, {}^{9}/_{11}, {}^{10}/_{11}$. $P^{Ta(1)} = {}^{1}/_{11}, ..., {}^{5}/_{11}$ yields the same structures since the roles of Ta(1) and Ta(2) are then simply interchanged. The numbers of Ta(1) and Ta(2) atoms will be used to label the models, so the 6–5 model refers to that with $P^{Ta(1)} = {}^{6}/_{11}$, and therefore $P^{Ta(2)} = {}^{5}/_{11}$. In Figure 1 the experimental mean intensities of each satellite order are compared with the square of the calculated Fourier amplitudes for each of the five models. The 6-5 and the 7-4 models are in best agreement with the experimental intensities and prove also to be the best in the subsequent refinements.

With the most probable intrasandwich cationic arrangements having been established, the relative orientation of the two sandwiches in the unit cell or, in other words, the correct space group symmetry had to be found. The reflection conditions observed in the diffraction pattern are, apart from the conditions due to the B centering, as follows: $0klm$, $k = 2n$; $0klm$, $k + m = 2n$.[30] Disregarding the few weak violations of these conditions, the (3 + 1)D superspace groups compatible with the symmetry are either $Bbmm(00\gamma)$ and $Bbm2(00\gamma)$ or $Bbmm(00\gamma)s00$ and $Bbm2(00\gamma)s00$. The latter two however, never lead to the supercell 3D space groups $Bbmm$ and $Bbm2$, whatever the value of the modulation phase t.[31] Therefore, the former two groups were chosen for refinement tests. It should be noted that the choice of these space groups fixes the position of the second sandwich with respect to the first one since the two sandwiches are connected by symmetry elements. However, the assumed superspace groups proved to be incorrect, since the R-factors remained very high. To obtain different stacking models, a space group without these symmetry elements had to be selected. $B2mm(00\gamma)$,[32] without any reflection conditions other than that from the B-centering, fulfills this requirement: the two sandwiches are not symmetry related. With this space group, another stacking could be chosen in better agreement with the stacking encountered in the other MA_xTe_2 compounds.

Both the 7-4 as the 6-5 models yielded satisfactory results in the subsequent refinements (see Table 2). The relatively large R-factors for the higher order satellite reflections are caused by the fact that they are inherently weak and therefore could not be measured with the same accuracy as the much stronger main reflections and first-order satellites. On the basis of the agreement factors the 7-4 model has to be preferred to the 6-5 model. A mixed model, i.e. one sandwich in the 7-4 mode and the other in the 6-5 mode, gave roughly the same R-factors as the 6-5 model. The 7-4 model will therefore be taken as the correct one, although the structural differences with the 6-5 model will be briefly addressed in the following discussion. The final refinement was stable for all atoms but for the Ge(2) atom that tended to drift away from its position within the Te-square. Difficulties in stabilizing the A position have also been encountered in other refinements of structures of MA_xTe_2 compounds.[24] They are related to stacking faults, e.g. shear domains, in the structure that primarily cause residual densities at empty M sites of the ideal structure. The drifting of the position of the A ion on refinement tries to cover these residual densities.

Details on the way refinements are performed for this type of commensurately modulated structures are described elsewhere.[23] Only reflections with $I \geq 2.5\,\sigma(I)$ have been used. The absolute configuration was checked by reversing the signs of the imaginary part of the anomalous dispersion terms. The results of the refinements have been compiled in Table 3. Some information on bond distances can be found in Table 4.

Table 2. Agreement Factors of the Refinements of the 7–4 and 6–5 Models[a]

		7–4 model		6–5 model	
reflcn order	no. of reflcns	R	R_w	R	R_w
0	536	0.074	0.081	0.080	0.089
1	798	0.070	0.071	0.090	0.101
2	398	0.159	0.168	0.167	0.161
3	84	0.357	0.444	0.324	0.470
4/5	61	0.417	0.495	0.412	0.517
overall	1877	0.095	0.094	0.106	0.109

[a] Note: The definitions of the R-factors are $R = \sum||F_o| - |F_c||/\sum|F_o|$ and $R_w = [\sum w(|F_o| - |F_c|)^2/\sum w|F_o|^2]^{1/2}$.

Discussion

Intrasandwich Structural Features. The structural features of $TaGe_{4/11}Te_2$ are at first sight not very different from those in the other MA_xTe_2 compounds were it not for the repetition length along c which is larger than has been seen thus far. Figure 2 presents projections of the two symmetry-unrelated sandwiches upon the planes $y = {}^{1}/_{4}$ and $y = {}^{3}/_{4}$, respectively. Figure 3 compares more schematically the single structure of one $TaGe_{4/11}Te_2$ sandwich with that of other compounds in the MA_xTe_2 series. The peculiar new feature of the structure of $TaGe_{4/11}Te_2$ is that whereas the tilting angle of the Ta–Ta bonds in the other MA_xTe_2 structures ($x = {}^{1}/_{3}, {}^{2}/_{5}, {}^{3}/_{7}$) is the same in a given row along c but changes sign from a row to the next one, it changes sign in $TaGe_{4/11}Te_2$ in the same row because of the presence of a mirror perpendicular to c.

Another difference is the larger concentration of faults (regions with "lone" Ta atoms, shaded in Figure 3) than in the other MA_xTe_2 compounds, viz. a diminishing fault concentration with increasing supercell size. Each sandwich in the structure of $TaGe_{4/11}Te_2$ contains four such faults per unit cell, of which two are of the same zigzag type as are found in the other MA_xTe_2 compounds. The other two faults, centered on the mirror planes perpendicular to c, are different since they contain only one lone Ta atom. They can, however, be thought as being created from the normal faults by a shear displacement as depicted in Figure 4. When the two half faults are combined, the original zigzag fault is regained. In this way, the 11-fold superstructure can be easily generated from the 3-fold superstructure at the cost of a $TaTe_2$ unit.

Considering again the five most probable intrasandwich cationic arrangements of Figure 1, we see that the 7-4 model is closest

(30) $\langle I/\sigma(I)\rangle = 3.93$ for 417 $0klm$ ($k = 2n$) reflections; $\langle I/\sigma(I)\rangle = 1.08$ for 399 $0klm$ ($k = 2n + 1$) reflections; $\langle I/\sigma(I)\rangle = 4.14$ for 406 $0klm$ ($k + m = 2n$) reflections; $\langle I/\sigma(I)\rangle = 0.95$ for 410 $0klm$ ($k + m = 2n + 1$) reflections.

(31) The possible 3D space groups for $Bbmm(00\gamma)s00$ are (see e.g. ref 22 for details on a similar derivation): $t = 0 \pmod{{}^{1}/_{22}} \rightarrow B2/m$; $t = {}^{1}/_{4} \pmod{{}^{1}/_{22}} \rightarrow B2mm$; else Bm_y. For $Bbm2(00\gamma)s00$ only Bm_y results.

(32) The generators used are $(E1|n_1,n_2,n_3,n_4)$, $(E1|n_1 + {}^{1}/_{2},n_2,n_3 + {}^{1}/_{2},n_4)$, $(m_x1|0,{}^{1}/_{2},0,0)$, and $(m,1|0,{}^{1}/_{2},0,0)$. Note the nonconventional position of the m_y mirror plane at $y = {}^{1}/_{4}$ to facilitate comparison with the other MA_xTe_2 compounds.

(33) Petříček, V.; Van der Lee, A. Manuscript in preparation, 1994.

Table 3. Final Results of the Refinements[a]

	Ta(1)	Ta(2)	Ta(3)	Ta(4)	Ge(1)	Ge(2)	Te(1)	Te(2)
P'_0	0.636364	0.363636	0.363636	0.636364	0.1818182	0.1818182	1.000000	1.000000
x	0.3140(9)	0.036(1)	0.688(1)	0.9692(9)	0.422(2)	0.588(2)	0.1688(6)	0.831576
y	0.25	0.25	0.75	0.75	0.25	0.75	0.1157(3)	0.8829(3)
z	0.00	0.00	0.00	0.00	0.271(3)	0.788(3)	0.50	0.50
$P'_{s,1}$	0.00	0.00	0.00	0.00	0.323552	0.329159	0.00	0.00
$P'_{c,1}$	0.587058	−0.587058	−0.587058	0.587058	−0.130619	−0.115768	0.00	0.00
$A'_{x,s,1}$	0.00	0.00	0.00	0.00	0.00	0.00	0.00	0.00
$A'_{y,s,1}$	0.00	0.00	0.00	0.00	0.00	0.00	0.00	0.00
$A'_{z,s,1}$	−0.066(1)	0.00	0.00	−0.086(1)	0.00	0.00	−0.012(1)	0.009(1)
$A'_{x,c,1}$	0.00	0.00	0.00	0.00	0.00	0.00	−0.037(1)	−0.0446(9)
$A'_{y,c,1}$	0.00	0.00	0.00	0.00	0.00	0.00	−0.0009(4)	−0.0002(4)
$A'_{z,c,1}$	0.00	0.00	0.00	0.00	0.00	0.00	0.00	0.00
$P'_{s,2}$	0.00	0.00	0.00	0.00	0.212404	0.191506	0.00	0.00
$P'_{c,2}$	−0.254169	0.254169	0.254169	−0.254169	−0.220184	−0.238581	0.00	0.00
$A'_{x,s,2}$	0.00	0.00	0.00	0.00	0.00	0.00	0.00	0.00
$A'_{y,s,2}$	0.00	0.00	0.00	0.00	0.00	0.00	0.00	0.00
$A'_{z,s,2}$	0.00	−0.057(2)	−0.064(2)	0.00	0.00	0.00	−0.004(2)	−0.007(1)
$A'_{x,c,2}$	0.010(1)	0.00	0.00	0.009(1)	0.00	0.00	0.009(1)	0.001(1)
$A'_{y,c,2}$	0.00	0.00	0.00	0.00	0.00	0.00	−0.0050(6)	0.0016(7)
$A'_{z,c,2}$	0.00	0.00	0.00	0.00	0.00	0.00	0.00	0.00
$P'_{s,3}$	0.00	0.00	0.00	0.00	0.097051	0.125735	0.00	0.00
$P'_{c,3}$	−0.067821	0.067821	0.067821	−0.067821	0.217481	0.202256	0.00	0.00
$A'_{x,s,3}$	0.00	0.00	0.00	0.00	0.00	0.00	0.00	0.00
$A'_{y,s,3}$	0.00	0.00	0.00	0.00	0.00	0.00	0.00	0.00
$A'_{z,s,3}$	0.030(2)	0.00	0.00	0.011(2)	0.00	0.00	0.007(18)	0.004(3)
$A'_{x,c,3}$	0.00	−0.023(2)	0.014(2)	0.00	0.00	0.00	−0.001(2)	0.012(1)
$A'_{y,c,3}$	0.00	0.00	0.00	0.00	0.00	0.00	−0.0002(8)	−0.0011(9)
$A'_{z,c,3}$	0.00	0.00	0.00	0.00	0.00	0.00	0.00	0.00
$P'_{s,4}$	0.00	0.00	0.00	0.00	0.150973	0.147505	0.00	0.00
$P'_{c,4}$	0.197931	−0.197931	−0.197931	0.197931	0.005472	0.032642	0.00	0.00
$A'_{x,s,4}$	0.00	0.00	0.00	0.00	0.00	0.00	0.00	0.00
$A'_{y,s,4}$	0.00	0.00	0.00	0.00	0.00	0.00	0.00	0.00
$A'_{z,s,4}$	0.015(3)	0.00	0.00	−0.029(3)	0.00	0.00	−0.006(2)	0.022(3)
$A'_{x,c,4}$	−0.006(2)	0.00	0.00	−0.002(2)	0.00	0.00	−0.021(1)	0.019(2)
$A'_{y,c,4}$	0.00	0.00	0.00	0.00	0.00	0.00	−0.0037(9)	−0.002(1)
$A'_{z,c,4}$	0.00	0.00	0.00	0.00	0.00	0.00	0.00	0.00
$P'_{s,5}$	0.00	0.00	0.00	0.00	0.017580	0.006262	0.00	0.00
$P'_{c,5}$	−0.099352	0.099352	0.099352	−0.099352	−0.048679	−0.051374	0.00	0.00
$A'_{x,s,5}$	0.00	0.00	0.00	0.00	0.002(4)	0.016(3)	0.00	0.00
$A'_{y,s,5}$	0.00	0.00	0.00	0.00	0.00	0.00	0.00	0.00
$A'_{z,s,5}$	0.00	0.044(1)	0.005(3)	0.00	−0.012(5)	0.033(5)	−0.022(2)	0.008(3)
$A'_{x,c,5}$	−0.015(2)	0.00	0.00	−0.010(2)	0.00	0.00	0.028(2)	−0.013(3)
$A'_{y,c,5}$	0.00	0.00	0.00	0.00	0.00	0.00	−0.0014(8)	−0.001(1)
$A'_{z,c,5}$	0.00	0.00	0.00	0.00	0.00	0.00	0.00	0.00

[a] Notes: A number of the zero entries in the table are required so by symmetry: $A^{Ta}_{x,s,n} = A^{Te}_{x,s,n} = A^{Ta}_{y,s,n} = A^{Ge}_{y,s,n} = A^{Te}_{y,s,n} = A^{Ta}_{y,c,n} = A^{Ge}_{y,c,n} = A^{Ta}_{z,c,n} = A^{Te}_{z,c,n} = 0$. Other amplitudes that are formally allowed by symmetry have been set to zero by application of the maximum determinant rule[33] to avoid convergement-inhibiting correlations. The values of the Fourier amplitudes of the occupation wave have been calculated to give a fully ordered distribution of cations according to the 7–4 model. Experimental standard deviations are within parentheses.

Table 4. Main Interatomic Distances in the Structure of $TaGe_{4/11}Te_2$[a]

	Ta–Ta	Ta–Ge	Ta–Te	Ge–Te	Te–Te(1)[b]	Te–Te(2)[b]	Te–Te(3)[b]
$\langle d \rangle$	2.846	2.833	2.873	2.751	3.928	3.792	3.763
$\sigma_{\langle d \rangle}$	0.110	0.111	0.138	0.151	0.152	0.207	0.130
d_{min}	2.711	2.620	2.631	2.456	3.734	3.383	3.647
d_{max}	2.981	3.013	3.189	2.987	4.176	4.191	4.098

[a] $\langle d \rangle$ is the mean of all closest contacts found in the structure; $\sigma_{\langle d \rangle}$ refers to the standard deviation of the mean, thus not to the usual crystallographic standard deviation; d_{min} and d_{max} are the minimal and maximal distance, respectively, found in each set. All distances are in Å. [b] Key: (1) Te–Te contacts through the van der Waals gap, i.e. joining two different sandwiches; (2) Te–Te contacts parallel to the layers, i.e. within one Te sheet; (3) Te–Te contacts through a sandwich, i.e. joining the two Te sheets constituting one sandwich.

to the arrangement of the other MA_xTe_2 compounds. The 6-5 model, which also resulted in quite good R-factors, does not have any complete fault but only 6 half-faults. The other three models contain Ta triplets besides a combination of half and complete faults.

The shear displacement not only generates a new ordering motif for the cations but also influences the bonding geometry. $TaGe_{4/11}Te_2$ exhibits a large distance variation (Table 4), whereas the $NbGe_{(1+n)/(3+2n)}Te_2$ (n = 0, 1, 2) compounds show very little variation between the different compounds. Te distances scale fairly well with those in $NbGe_{(1+n)/(3+2n)}Te_2$ and in $TaSi_{1/3}Te_2$, but metal to anion distances differ. The shortest Ta–Te distances (2.631, 2.649, 2.650, 2.658 Å) are unusually short but not improbable.[34] Because of these short distances, $TaTe_6$ trigonal prisms are more distorted in $TaGe_{4/11}Te_2$ than in other MA_xTe_2 compounds. Ge atoms are more displaced from the center of the Te_4 square than in other MA_xTe_2 structures, the shortest Ge–Te

(34) Shortest Ta–Te distances (Å): $Ta_3Pd_3Te_{14}$, 2.644(2); $Ta_4Pd_3Te_{16}$, 2.662 (8); $TaIrTe_4$, 2.646(12).

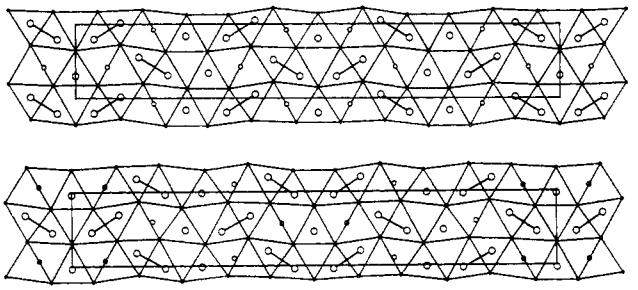

Figure 2. Projected structure of the two symmetry-unrelated sandwiches in the structure of $TaGe_{4/11}Te_2$ on the planes $y = {}^1/_4$ (top) and $y = {}^3/_4$ (bottom), respectively. Te atoms are depicted as small open circles; Nb atoms are indicated by large open circles, and Ge atoms, by medium-sized open circles. The axes are as in Figure 1.

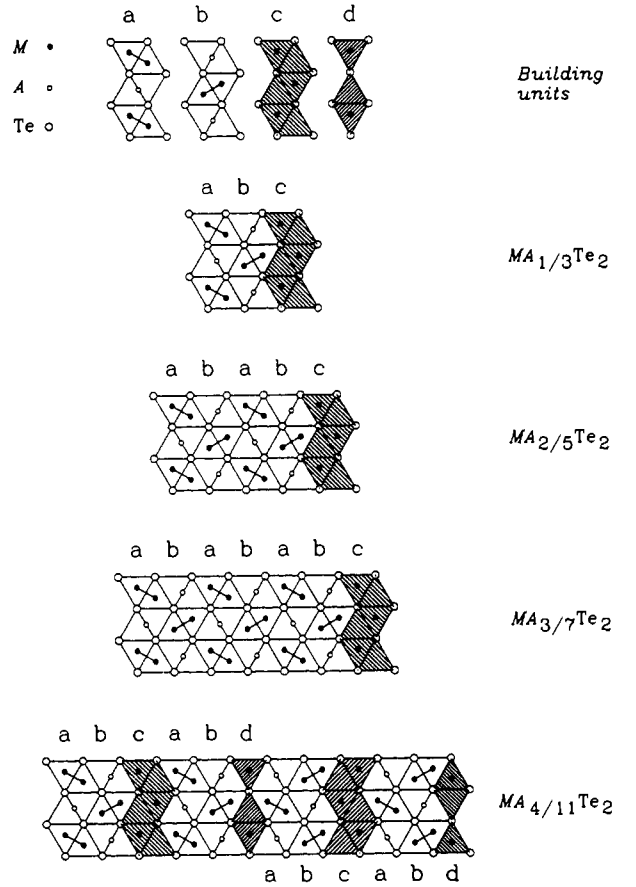

Figure 3. Comparison of intrasandwich cationic arrangements for the 3-, 5-, 7-, and 11-fold superstructures in the MA_xTe_2 series. The displacive modulations have not been taken into account. The axes are as in Figure 1.

distances being 2.456 and 2.581 Å. The former distance is probably too short as indicated by the difficulty in stabilizing the Ge(2) position.

Intersandwich Pinning. The clue that led to the succesful structure solution is the correct stacking of the two sandwiches in the unit cell. Figure 5a–c gives schematic representations of the intrasandwich cationic arrangements for the proper stacking of *B2mm*(00γ) (Figure 5a,b) and of the incorrect stacking that is imposed by the symmetry operations of *Bbmm*(00γ) (Figure 5a,c). It should be emphasized that in both cases the stacking of the successive Te sheets occurs in the AA/BB mode as for the majority of the structures throughout the MA_xTe_2 series. Thus, it seems that it is the cationic stacking rather than the anionic stacking that determines the stability of the compound.

It is easily seen from Figure 5 that the correct structure cannot be described, not even approximately, in the centrosymmetric space group *Bbmm*(00γ). Note, however, that the way the lost

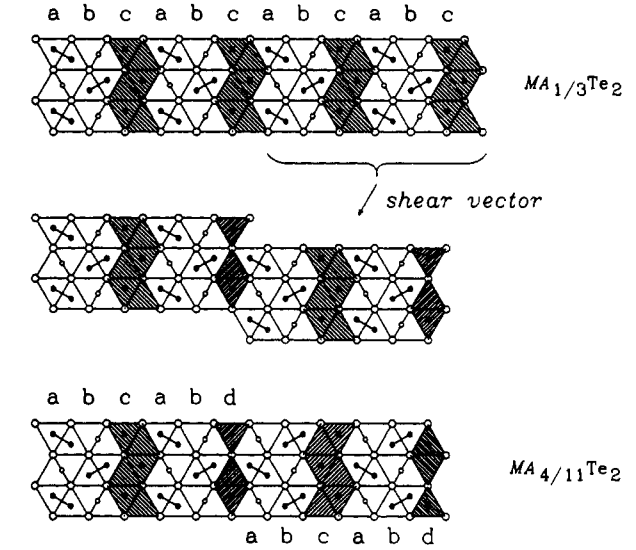

Figure 4. Creation of the 7-4 model for $TaGe_{4/11}Te_2$ from the 3-fold superstructure by a shear displacement of two complete units. The a–d symbols refer to the same building units as in Figure 3. The axes are as in Figure 1.

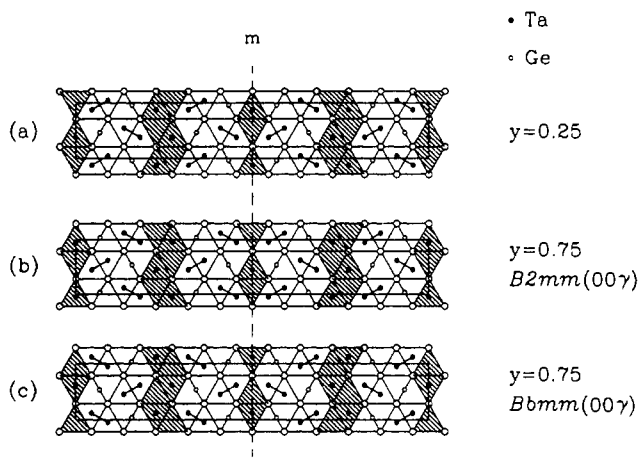

Figure 5. The comparison of the two different stacking models for $TaGe_{4/11}Te_2$ according to the superspace groups *B2mm*(00γ) and *Bbmm*(00γ). The common sandwich at $y = 0.25$ is depicted in (a), the sandwich at $y = 0.75$ as was found in the *B2mm*(00γ) refinement is in (b), and the sandwich at $y = 0.75$ as is generated from that at $y = 0.25$ by the symmetry operations of *Bbmm*(00γ) is in (c). The axes are as in Figure 1.

inversion operator acts can be redefined in the case of Ta(1) and Ta(2): the operator reverses not only the coordinates but it also "reverses" the occupation probability. In mathematical terms this means that

$$\Re_T P = 1 - P$$

Unfortunately, this extended definition cannot be used for Ge. Instead of an inversion center, it is now approximately a translation of $\mathbf{a}/3 + \mathbf{b}/2$ that connects the two sandwiches. A refinement of a model that constrains the two sandwiches in this way was not succesful; thus, the translation is indeed only approximate.

It was earlier shown that there exists a relation between the spacing of the faults in two successive sandwiches in terms of the basic repetition length $\mathbf{c}_b$ for the $NbGe_{(1+n)/(3+2n)}Te_2$ compounds. In order to obtain a stable structure, this spacing has to be $(l + {}^1/_2)$, l = odd. For $TaGe_{4/11}Te_2$ this empirical rule does not hold; the spacing is always exactly zero regardless the model. The difference is caused by the different symmetry for $NbGe_{(1+n)/(3+2n)}Te_2$ and $TaGe_{4/11}Te_2$, respectively. The symmetry

of the former phases can never lead to a zero fault spacing, whereas the symmetry of $TaGe_{4/11}Te_2$ never yields a $(l + {}^1/_2)$ spacing.

Electronic Transfer Versus Structural Features. As already stated in the Introduction, the loss of one Ge atom, in comparison with what is expected from the general formula $MA_{(1+n)/(3+2n)}Te_2$, implies an enhanced charge transfer of two extra electrons from the Te p-orbitals to the Ta d-block bands. It was earlier shown that a charge transfer of one electron corresponds with the occurrence of one normal fault per sandwich per unit cell. In addition, two short intersandwich Te–Te contacts are associated with each fault.[22] These Te–Te contacts have been related to the charge-transfer process by extended Hückel tight-binding band structure calculations.[25]

The present structure determination of $TaGe_{4/11}Te_2$ shows that this concept can be generalized: the charge transfer of three electrons requires the presence of three normal faults per sandwich per unit cell. In the structure of $TaGe_{4/11}Te_2$ one fault is split, so that there are indeed $(2 + 2 \times {}^1/_2) = 3$ normal faults. Again, the short intersandwich Te–Te contacts associated with the faults are present, the shortest intersandwich Te–Te distances lying between 3.73 and 3.80 Å, in perfect agreement with the corresponding distances of other compounds throughout the MA_x-Te_2 series. This is in good accord with the shortest intersandwich Te–Te distances found in another ternary telluride, viz. 3.734, 3.746, and 3.776 Å in $TaIrTe_4$, with a quite distinct intrasandwich cationic arrangement.[12] Another similarity with the other MA_x-Te_2 compounds is that the Te atoms associated with the short contact at the normal faults are slightly displaced inward the sandwich as for the $NbGe_{(1+n)/(3+2n)}Te_2$ compounds. The geometry of the half-faults is, however, different: the short contact Te atoms protrude out of the sandwich.

Regarding the complete faults, the Te atoms associated with the short intersandwich contacts are always located at the "outer" corner of the fault. Since the sandwiches are fairly rigid, those corners are the only points where the sandwiches can be pinned upon each other in order to adjust the electron counting of the compound. This suggests that the faults play a crucial role in the structural response to the electronic stabilization. Indeed, faults are encountered in all MA_xTe_2 compounds except in $NbSi_{1/2}Te_2$,[19] where Te^{2-} need not to be oxidized in order to meet the oxidation state requirements of Nb^{3+} and Si^{2+}. One could equally well suggest that the relative orientation of the cationic distribution in two successive sandwiches is responsible for the stabilization, since the position of the faults is directly related to that of all cations.

Although the electron transfer per Te atom changes continously from 0 in $NbSi_{1/2}Te_2$ to ${}^1/_3$ in $MA_{1/3}Te_2$, the associated Te–Te contact distances remain surprisingly constant. This probably stems from the fact that the electron donation to the system, or more precisely, the position of the Fermi level, is controlled via the amount of A in MA_xTe_2. This makes possible the setting up of superstructures with constant intersandwich Te–Te contact lengths rather than adjusting the contact length with varying charge transfer. The latter applies better to the study of Mar et al.[12] and Jobic et al.,[13] who use heterocharge substitution of cations to control the electron count. It remains surprising that the band structure calculations give equal oxidation states for all M cations, whether they are paired or not.[20, 25] It is tempting to assign different oxidation states to the paired M atoms on the one hand and the lone atoms on the other hand, implying a more complicated charge-transfer scheme than presented here. New experiments and calculations are under way to clarify these charge-transfer processes.

Concluding Remarks

The unraveling of the crystal structure of $TaGe_{4/11}Te_2$ has shown that the structural response to the charge transfer process in MA_xTe_2 compounds is possible in more ways than previously thought. Instead of a setting up of an incommensurate sequence of $n = 0$ and $n = 1$ $TaGe_{(1+n)/(3+2n)}Te_2$ blocks as is the case for $TaSi_{0.360}Te_2$,[21] the structure is commensurate with the basic lattice but contains a concentration of faults of lone Ta atoms larger than normally found in commensurate MA_xTe_2 compounds. The question why the system responds with a commensurate rather than with an incommensurate sequence cannot be answered on basis of the present results. Also unanswered is why only $TaGe_{4/11}Te_2$ seems to exist, whereas the 3-fold superstructures of $TaSi_{1/3}Te_2$, $NbSi_{1/3}Te_2$, and $NbGe_{1/3}Te_2$ are easily made.

Although the 7-4 model was taken as the correct one for the intrasandwich cationic arrangement, the 6-5 model cannot be completely excluded, because the R-factors for the final refinements are only slightly higher. Additional techniques, such as HREM or STM/AFM, might be fruitful to make a decisive choice between the two models.

Acknowledgment. The research of A.v.d.L. has been made possible by a grant from the Conseil Régional des Pays de la Loire, and that of V.P., by the Grant 202/93/1154 from the Grant Agency of the Czech Republic.

Supplementary Material Available: Tables listing recording conditions, crystallographic data including supercell atomic coordinates, bond distances, and thermal parameters (9 pages). Ordering information is given on any current masthead page.